Martian atmospheric tides revealed from MAVEN and MCS Observations

Chengyun Yang[1,2], Tao Li*[1,2], Mengzhen Yuan[1] and Zhaopeng Wu[3]

[1] CAS Key Laboratory of Geospace Environment, School of Earth and Space Sciences, University of Science and Technology of China, Hefei, China.

[2] CAS Center for Excellence in Comparative Planetology, University of Science and Technology of China, Hefei, China.

[3] Key Laboratory of Earth and Planetary Physics, Institute of Geology and Geophysics, Chinese Academy of Sciences, Beijing, China.

Corresponding author: Tao Li, litao@ustc.edu.cn

Key Points:

- The thermal tides are derived from temperature observation by Imaging Ultraviolet Spectrograph on Mars Atmosphere and Volatile Evolution.
- The strong tides in the upper atmosphere are migrating tides (DW1 and SW2), and nonmigrating diurnal eastward wavenumber 2 tide (DE2).
- The DE2 exhibits characteristics of propagating from the lower to the upper atmosphere of Mars.

Abstract

Utilizing atmospheric temperature observed from Mars Years 33 to 36 by the Imaging Ultraviolet Spectrograph (IUVS) onboard the Mars Atmosphere and Volatile Evolution (MAVEN), we derive the diurnal and semidiurnal thermal tides from 90 to 160 km. The seasonal variations of diurnal (DW1) and semidiurnal (SW2) tides in the thermosphere and mesosphere, observed by the Mars Climate Sounder (MCS), along with vertical phase velocities, indicate different sources for the migrating tide in the lower and upper atmosphere. The seasonal variation of diurnal eastward wavenumber 2 (DE2) tide in the thermosphere corresponds well to its counterpart in the lower atmosphere. Vertical phase velocities indicate that the DE2 propagates upward from the lower atmosphere to ~150 km, except near the perihelion (solar longitude 210° to 270°). The upward propagation of this DE2 tide could potentially impact the vertical coupling between the Martian lower and upper atmosphere.

Plain Language Summary

Atmospheric thermal tides are perturbations caused by the absorption of solar radiation in the atmosphere, a phenomenon in Earth's and other planetary atmospheres. The vertical propagation of tides plays a crucial role in transporting energy and momentum vertically within the atmosphere. Observing atmospheric temperatures at different local times makes it possible to determine the amplitude and propagation characteristics of various tidal components. Based on data from different satellites, this study investigates the characteristics of tidal amplitude and propagation on Mars. Among the various tidal components examined, only the diurnal eastward propagating wavenumber 2 (DE2) tide exhibits apparent upward propagation from the lower atmosphere to above 150 km, with its seasonal variation patterns agreeing with those in the lower atmosphere. As Mars has weaker gravity and a lower exobase altitude than Earth, the vertical propagation of tides may directly transmit energy from lower atmospheric activities to the upper layers of the Martian atmosphere, influencing the atmospheric escape rate.

1 Introduction

As a planetary-scale gravity internal wave, atmospheric solar tides can significantly influence diurnal and semidiurnal variations of the density, temperature, pressure, and wind in the Martian atmosphere (Chapman & Lindzen, 1987; Forbes, 2013; Forbes et al., 2020). Given their characteristics of vertical propagation and tendency to grow with height, atmospheric tides play a crucial role in transporting momentum and energy from the lower atmosphere to higher altitudes, even to the edge of the space (Angelats I Coll et al., 2004; England et al., 2016, 2019; Forbes et al., 2002; Moudden & Forbes, 2015). In addition, the tides can influence water vapor transport by driving mesospheric meridional circulation and redistributing the minor chemical constituents (Shaposhnikov et al., 2019; Wu et al., 2020) or influencing Jeans escape of hydrogen into space through wave-induced perturbations in temperature and density in the thermosphere and near the exobase (Yiğit, 2021, 2023). Understanding the current state of atmospheric tides on Mars is crucial for unraveling the coupling mechanisms from the lower Martian atmosphere to the space environment, elucidating atmospheric escape processes, and ultimately comprehending the habitability history of Mars.

Since Hanel et al., (1972) pioneered the study of Martian atmospheric tides through temperature observations from the Infrared Spectroscopy Experiment on Mariner 9, the characteristics of the atmospheric tides on Mars have been unveiled with subsequent observations and model studies. Forbes et al. (2002) studied the vertical propagation of nonmigrating diurnal and semidiurnal tides through the GCM model and the Global Scale Wave Model for Mars (Mars GSWM). Wilson. (2002) used density data from the Mars Global Surveyor (MGS) accelerometer to discern wave 2 and wave 3 structures in the upper atmosphere of Mars, associating them with the diurnal eastward wavenumber 2 (DE2) and semidiurnal eastward wavenumber 1 (SE1) tides in the middle and low latitudes. Withers et al. (2011) investigate the DE1 and DE2 non-migrating tides between 70 and 120 km based on data from the Spectroscopy for Investigation of Characteristics of the Atmosphere of Mars (SPICAM) ultraviolet spectrometer onbaord Mars Express. Recently, Mars Climate Sounder (MCS) instrument onboard Mars Reconnaissance Orbiter (MRO) has implemented a multi-local time observational strategy (Kleinböhl et al., 2009), enabling concurrent measurements of atmospheric temperature and dust, which offers opportunities to ascertain the climatology and variation of the thermal tides (Lee et al., 2009; Wu et al., 2020, 2021). Forbes et al. (2020)

derived the climatology of migrating (DW1, SW2) and non-migrating (DE3, DE2, DE1, SE1, S0, and SW1) tides at 76 km from Multiyear MRO/MCS measurements, the amplitude and structure of which corresponds well with those from Mars Climate Database (MCD).

The Mars Atmosphere and Volatile EvolutioN (MAVEN) mission, which is designed to study the structure and escape of the Martian atmosphere, provides observation of the upper atmosphere and magnetosphere of Mars (Jakosky et al., 2015). Based on the temperature and density observation from stellar occultation of the Imaging Ultraviolet Spectrograph (IUVS) aboard MAVEN, recent studies investigated diurnal thermal tide (Gupta et al., 2022) and the wave-3 structure in the upper atmosphere on Mars (Fu et al., 2023). As suggested by previous work, there is no signatures of vertical propagating diurnal thermal tide discovered in the upper mesosphere/lower thermosphere (~80 to 160 km) of Mars, which are inconsistent with the MCD predictions (Gupta et al., 2022). Thus, the connection between the diurnal and semidiurnal tide in the lower atmosphere and those in the thermosphere remains unclear.

In pursuit of a deeper understanding of thermal tidal dynamics and vertical coupling between the lower and the upper atmosphere on Mars, this study elucidates the seasonal variations and vertical structures of both migrating and non-migrating atmospheric tides—from the troposphere to the thermosphere through a collaborative analysis of temperature data obtained from MRO/MCS and MAVEN/IUVS.

2 Data and Methods

2.1 MAVEN/IUVS

In this study, we derived the migrating and non-migrating tides within the upper atmosphere (90-160 km), utilizing limb observations facilitated by the IUVS instrument onboard the MAVEN spacecraft. MAVEN mission is committed to scrutinizing the contemporary conditions of the Martian upper atmosphere and ionosphere, which was launched in November 2013 and successfully achieving Martian orbit by October 2014. The mission is poised to enhance our understanding of atmospheric escape and the evolution of Martian climatology (Jakosky et al., 2015). The concrete working mechanism of IUVS can be referred to McClintock et al. (2015). Stellar occultation observations by the MAVEN/IUVS are executed in dedicated bimonthly “campaigns” which provide profiles of local densities, temperature, and pressure for different local times (Gröller et al., 2018; Jakosky et al., 2015; McClintock et al., 2015). Out of a total of 3,003 occultations since March 2015, 47% occurred during the daytime, which have been contaminated by stray light and cannot be utilized in most analyses (Jiang et al., 2019; Nakagawa, Jain, et al., 2020; Nakagawa, Terada, et al., 2020). By utilizing an improved algorithm, Gupta et al. (2022) have broadened the data set's usability of both daytime and nighttime variations for mission-wide investigations (covering Martian years (MYs) 33–36) in the Martian upper mesosphere/lower thermosphere (~80 to 160 km). This reprocessed dataset were adopted to derive the diurnal and semidiurnal tide in this study.

2.2 MCS datasets

This study utilizes the version 5 MCS dataset from the Planetary Data System. Over eight Martian years (MYs 28–36), MCS has systematically measured thermal emissions within the Martian atmosphere through both limb and on-planet perspectives. Operating at approximately 3 a.m./3 p.m. during 14 orbits within each sol, MCS covers an extensive latitudinal range from ~85◦S to ~85◦N. The retrieved MCS data is then interpolated across 105 vertical pressure levels, ranging from the planetary surface to ~80 km, with an effective vertical resolution of ~5 km (McCleese et al., 2007). Since September 2010, the MCS has adopted a "cross-track" observational strategy, which entails adjusting its azimuth actuator to observe the limb at angles of 90◦ to the left or right of the orbital direction. The specific observational angle allows for an additional local time observation during both the ascending and descending sections of the orbit (Kleinböhl et al., 2009). The "cross-track" observations have been intermittently carried out since MY 30. Each observational sequence is dedicated to covering the solar longitude (Ls) range of approximately 10–20◦, except for one full year in MY 33 (Wu et al., 2020).

2.3 Fitting the tides

According to different zonal wave numbers and frequencies, the atmospheric thermal tides can be expressed as the function of universal time and longitude:

$$x = A(z,\theta)\cos[n\Omega t + s\lambda + \Phi(z,\theta)] \quad (1)$$

where n is the frequency of the oscillation (n = 1,2 corresponds to diurnal and semidiurnal tides respectively), s is the zonal wave number (s > 0 corresponds to westward propagating tides, s < 0 corresponds to eastward propagating tides), z is altitude, θ is latitude, t is the universal time, Ω is the planetary rotation rate, λ is the longitude, A and φ are the amplitude and phase of the individual tidal mode. Generally, a tidal component is designated based on its frequency, zonal wave number, and propagation direction. For instance, a diurnal tide propagating eastward with a zonal wave number of 2 is referred to as DE2. The expression of the tides can be represented as:

$$x = A(z,\theta)\cos[(s-n)\lambda + \Phi'(z,\theta)] \quad (2)$$

when observed within the fixed local time frame. Through the collection of temperature observations at diverse locations during various local times, including both daytime and nighttime periods, it becomes feasible to employ fitting procedures to ascertain the amplitude and phase of the tides with different wave numbers and periods.

To obtain sufficient coverage of data in the longitude and local time required by tidal fitting, we first bin the temperature profiles from MAVEN/IUVS within a solar longitude span of 60° and a latitude span of 30° from all the Martian years. Only bins meeting the following two criteria are considered for fitting distinct tidal amplitudes and phases: 1) The bin must contain observations at more than four distinct local times, covering both daytime and nighttime, with the largest gap between adjacent local times being less than 8 hours. 2) there must be six or more distinct longitude observations for a specific local time observation, and the maximum gap between adjacent longitude observations should not exceed 90°.

An example of the data binning strategy in longitude–local time dimensions is shown in **Figure 1a**. Within the latitude range of 15°S to 15°N and the Ls range of 30°-90°, 101 temperature measurements at 130 km altitude were conducted across six campaigns spanning from MY 33 to 36, including a broad range of longitudes and various local times during both day and night. As the local time interval is smaller than the period of semidiurnal tides, the diurnal and semidiurnal tides can be determined by fitting. Considerable variations in atmospheric temperatures are evident at distinct local times within the thermosphere, spanning the altitude range of 90 km to 160 km (**Figure 1b**), implying the activity of the diurnal tides.

Subsequently, the temperature data at a specific altitude is fitted using harmonics, with longitude serving as the variable, enabling the determination of amplitude and phase for each wave structure. Fitting results within the latitude of 15°S to 15°N and Ls of 30°-90°are shown in

Figure 1c. The seasonal variation and meridional structure of tidal amplitude and phase can be obtained by repeating the fitting process for each latitude range and Ls bin. In accordance with the methodology outlined by (Wu et al., 2020), the amplitude and phase of diurnal and semidiurnal tides can be derived from the temperature data observed by the MCS through a 2-dimensional nonlinear least squares fitting procedure involving local time and longitude. Additional specifics regarding the fitting methodology for the estimation of tidal information are elaborated in (Wu et al., 2022).

3 Results

As depicted in **Figure 1c**, within the altitude range of 100 to 130 km, three tidal modes of migrating diurnal tide (DW1), migrating semidiurnal tide (SW2), and nonmigrating diurnal eastward wavenumber 2 (DE2) manifest notable amplitudes in 15°N-15°S during the Ls range from 30° to 90°. The DW1 attains its maximum amplitude of 15-20 K at ~120 km, coinciding with the day/night difference in the mesopause and lower thermosphere region (Gupta et al., 2022). The SW2 reaches its maximum amplitude of ~25 K below the altitude of 110 km but weaker above 120 km. The DE2 is most active with the peak of amplitude over 15 K at 120 km. Above 100 km, the annual mean tropical DE2 amplitude stands out as third most pronounced mode besides DW1 and SW2 (**Figure S1**). The significant thermospheric DE2 tide is consistent with previous studies (e.g. Fu et al., 2023).

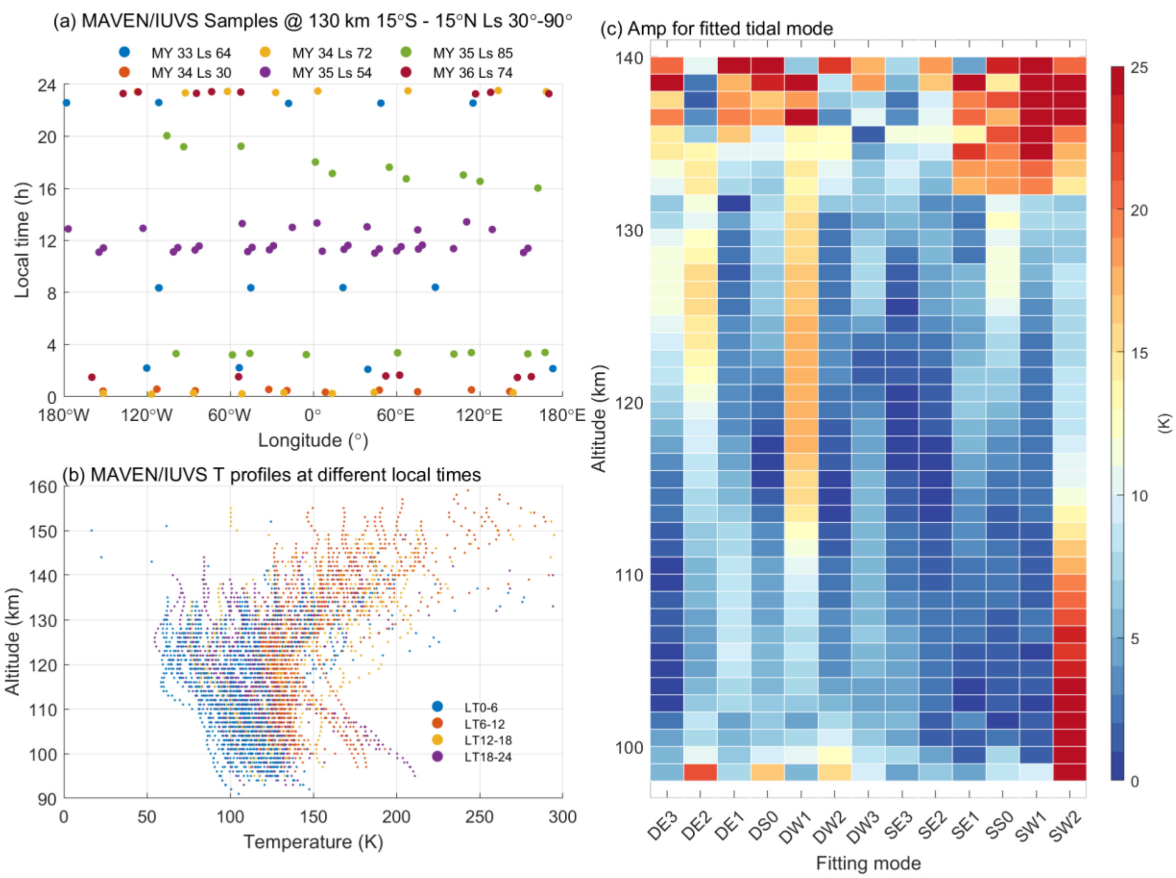

Figure 1. (a) the longitude and local time distribution of the MAVEN/IUVS sampling for temperature at 130 km from Ls 30°- 90°, latitude range of 15°S-15°N. (b) the temperature profiles at different local time and altitude from Ls 30°- 90°. (c) Amplitude for different tide modes fitted from the temperature profiles observed by MAVEN/IUVS from Ls 30°- 90°.

The variability of DW1 tidal amplitudes across diverse latitudes and solar longitudes throughout the whole Martian year is derived from fitting the temperature of multi-year MAVEN/IUVS stellar occultation observations at altitudes of 135 km and 100 km, respectively, as depicted in **Figures 2a** and **2b**. **Figure 2c** illustrates the seasonal variations of the DW1 mean amplitude at 75 km derived from MRO/MCS data covering MY 33 to 36 years.

The seasonal variations of DW1, SW2, and DE2 tides are significant in the Martian mesosphere and thermosphere. At 135 km, the amplitude of the DW1 tide estimated from the MAVEN/IUVS temperature is most significant in the southern hemispheric mid-latitudes near the spring equinox (Ls = 0°). In contrast, the amplitudes are weaker near the equator (**Figure 2a**). At 100 km, the amplitude of the DW1 tide is more prominent during the first half of the MY and weaker during the second half (**Figure 2b**). The mesospheric DW1 tide at 75 km, derived from MRO/MCS observations, exhibits greater amplitude near the equator, with two peaks manifesting in the Ls range of 120-180° and near 300°, respectively (**Figure 2c**). The amplitude of the DW1 shows inconsistent seasonal variations and meridional distributions at lower and higher altitudes, indicating that the DW1 tide in the mesosphere and thermosphere could driven by different sources, which agrees with the solar-controlled diurnal temperature variation in the thermosphere as suggested by (Gupta et al., 2022).

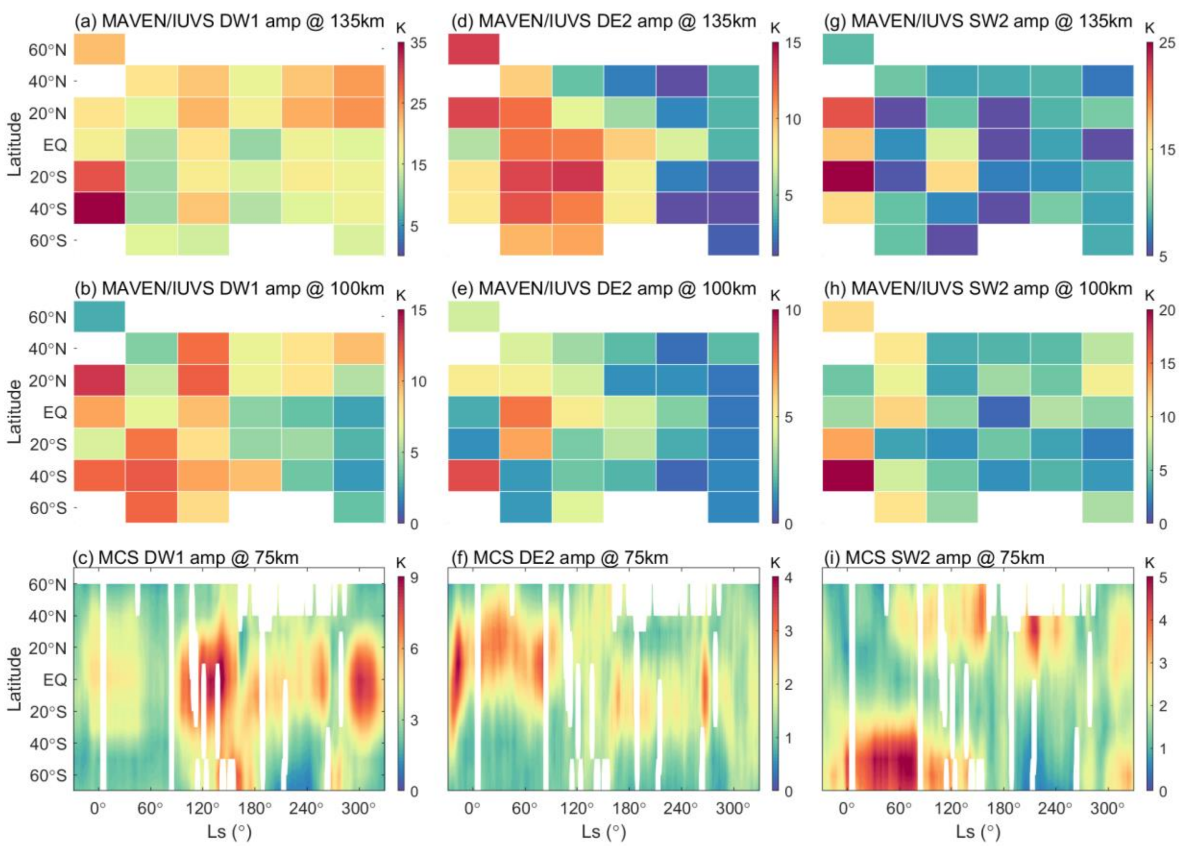

Figure 2. Seasonal variation of tidal amplitude derived from MAVEN/IUVS for DW1 (a, b), DE2 (d, f), SW2(g, h) at 135 km (upper panel) and 100 km (middle panel). The amplitudes for corresponding tidal components at 75 km during MY33-MY36 derived from MCS observation are presented in the lower panel (c, f, i).

As shown in Figures 2d and 2e, the DE2 amplitudes maximize in the tropical regions in the thermosphere. The amplitudes are significantly larger during the northern spring and summer (Ls = 300° to Ls = 150°) as compare to the northern autumn and winter (Ls = 150° to Ls = 300°). The seasonal and latitude pattern of mesospheric DE2 amplitude is similar to that in the thermosphere. At 100 km and 135 km (**Figure 2g and 2h)**, the SW2 amplitude attains its peak near the northern spring equinox (around Ls = 0°). The mesospheric SW2 has the largest amplitude in the middle and high latitudes around the winter solstices in both the northern and southern hemispheres (**Figure 2i**), which is different from that in the thermosphere.

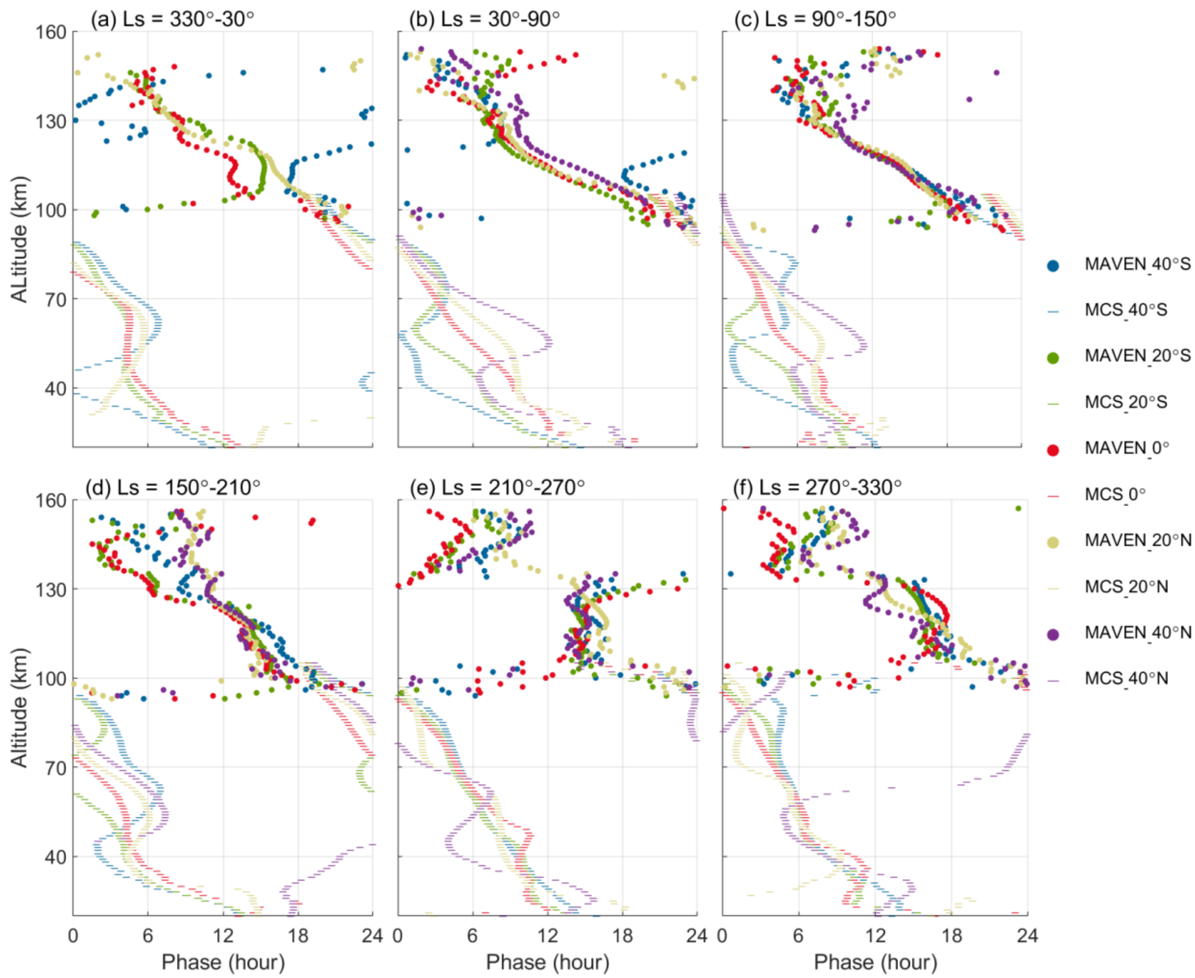

Figure 3. The vertical structure of the DE2 phase from 90 to 160 km derived from MAVEN/IUVS (dots) and from 20 to 100 km derived from MCS (bars) during MY33-MY36 at different latitudes and solar longitudes.

According to the theory for vertically propagating gravity waves, the wave phase progression in vertical is opposite to wave propagation of energy and momentum. Therefore, by tracking the vertical phase variation, one can estimate the vertical direction of tidal propagation and the potential altitude of the excitation source. Among the 14 tidal modes in the tropics, only DE2 exhibits a clear downward phase progression, indicating the upward propagation of wave energy and momentum (green line in **Figure S2b**). The DW1 phases progress upward indicates downward wave propagation within the altitude range of 100 to 160 km. This further suggests the diurnal tidal source in the thermosphere above 160 km, consistent with the dominant solar control over diurnal temperature variations due to the short radiative time constant (Gupta et al., 2022). On the other hand, the phase variation of the SW2 tide is insignificant with altitude in the thermosphere, which suggests that the SW2 is likely trapped above 100 km.

To further investigate the vertical propagation characteristics and potential excitation sources of the DE2 tide, **Figure 3** illustrates the multi-year averaged phase of DE2 tide extracted from MAVEN/IUVS (90-160 km) and MRO/MCS (30-100 km) temperature observations in 6 Ls ranges and 5 latitude ranges. By examining the vertical propagation characteristics of tides, we can estimate potential tidal excitation sources. At the northern spring equinox (Ls 330°-30°), DE2 propagate downward below 60 km and upward above 70 km unitl ~140 km in the tropical region and northern hemisphere, suggesting the excitation source of DE2 likely located near 60 km (**Figure 3a**). From Ls 30° to 210°, DE2 propagates upward from the mesosphere into the thermosphere in mid-latitudes near the equator (**Figure 3b** to **3d**). However, the phase structure in the lower atmosphere varies significantly with latitudes. The tidal excitation source, which could be excited by the heating or the nonlinear interaction from other tidal components (Forbes et al., 2020), near the equator can be traced to altitudes below 40 km, while in mid-latitudes, potential tidal excitation sources vary in the altitude range of 50-100 km..

Near perihelion (Ls 210°-270°, **Figure 3e**), the DE2 phase progress downward below 100 km, while progress upward above 130 km. The phase of DE2 remain at 15 local time between 100 and 130 km. This vertical phase structure indicates that the DE2 propagate upward from the lower atmosphere into the mesosphere and then is suppressed in the lower thermosphere, which could potentially contribute to the decreased DE2 amplitude above 130 km (**Figure 2d and 2e**). From Ls 210° to 270° (**Figure 3f**), the vertical phase structure of the DE2 indicates upward propagation of the tide within the range of 100-140 km, particularly in the mid-latitudinal regions of the Northern Hemisphere (yellow and purple dots in **Fiugre 4f**). In summary, the DE2 tide exhibits clear upward propagation from the lower atmosphere (below 70 km) to the thermospheric region (above 140 km) throughout the whole Martian year, except the period near the perihelion (Ls 210°-270°).

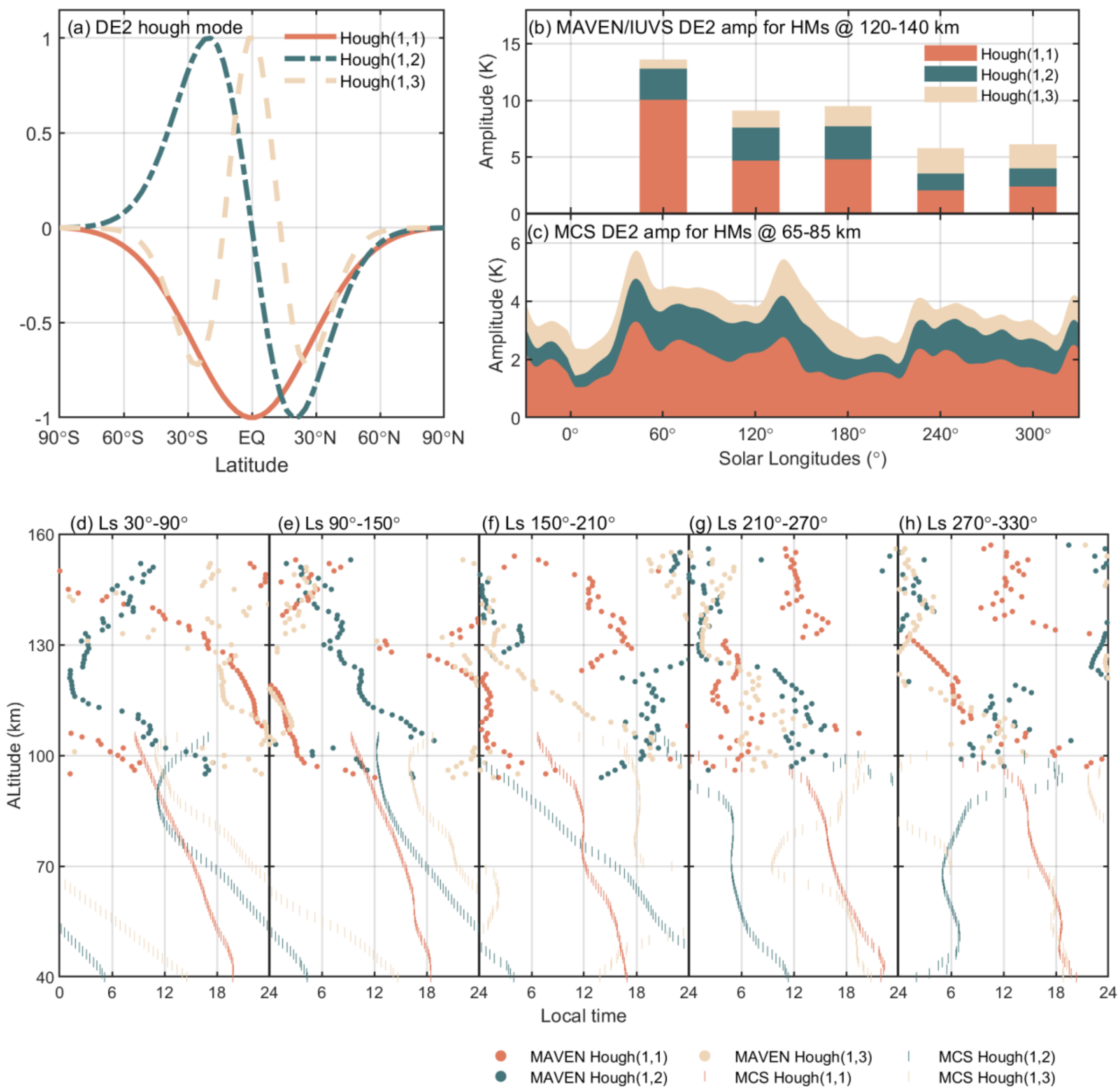

Figure 4. (a) the DE2 Hough mode; (b) the amplitudes for the first three DE2 Hough modes at 120-140 km from MAVEN/IUVS at different solar longitudes (each corresponds to a 60° Ls span); (c) the amplitudes for the first three DE2 Hough modes at 65-85 km from MCS; (d)-(h) the phase for DE2 Hough modes at different solar longitudes from MAVEN/IUVS temperature (dots) and from MRO/MCS temperature (short vertical line).

In accordance with classical tidal theory, the latitudinal structure of a tide characterized by a specific wavenumber and period can be represented through an expansion of orthogonal Hough functions. These functions serve as eigenfunction solutions to Laplace's tidal equation

(Chapman & Lindzen, 1987; Forbes et al., 2020). The DE2 tide could be determined by the variability of the first three Hough functions (**Figure 4a)**. By applying the Hough decompositions on the DE2 latitudinal structure within the latitude range from 55°S-55°N, the seasonal variability of amplitude for each DE2 Hough mode from 120 km to 140 km is presented in **Figure 4b**. Due to insufficient MAVEN/IUVS data in the range of Ls 330° to 30° between 25°N and 55°N, a Hough decomposition was not performed for the DE2 tide during this period. The (1, 1) mode exhibits a maximum amplitude of ~10K near the aphelion (around Ls = 60°) and notably diminishes with an amplitude of 2-3 Knear the perihelion (Ls = 240°-300°). Concurrently, the amplitude of the first antisymmetric (1, 2) mode is ~3K in the first half of a Martian year but decreases to ~1 K near perihelion. The amplitude of the (1,3) mode is less than 1K near the aphelion and increases gradually to ~3 K near the perihelion.

The seasonal variation of the (1, 1) mode, averaged from 65 to 85 km (**Figure 4c**), corresponds with the upper atmospheric pattern, exhibiting stronger amplitude during the first half of the Martian year. Meanwhile, the antisymmetric (1,2) mode has a weaker amplitude near the equinox compared to that near the solstice. The amplitude of the (1,3) mode remains similar during different Ls.

By examining the vertical phase structures of different modes (**Figure 4d to 4h**), we can further investigate the vertical propagation characteristics and the connection of DE2 seasonal variations between the mesosphere and the thermosphere. Near aphelion (**Figure 4d**), the (1, 1) mode exhibits continuous upward propagation from 40 km to above 150 km. The upward propagation of the (1, 2) mode reaches only 120 km, while the (1, 3) mode propagates upward until 110 km. During Ls 90°-150° (**Figure 4e**), the (1, 2) mode becomes the most prominent upward propagating mode. From Ls 150° to 330° (**Figure 4f to 4h**), the upward propagation of both (1,1) and (1,2) modes are suppressed above 100 km. The (1, 3) mode is enhanced from 80 km to above 130 km from Ls 150° to 270°. As a result, the amplitude of the (1, 3) mode experiences a noticeable enhancement in the thermosphere although its amplitude remains unchanged in the mesosphere. Since Ls 270°, the (1, 1) mode resumes upward propagation from the lower atmosphere to ~130 kilometers, while the upward propagation of the (1, 2) mode is unclear in the thermosphere.

4 Summary and Discussion

This study utilized temperature data recorded by MAVEN/IUVS, including both daytime and nighttime data, to fit 14 tidal components, including diurnal and semidiurnal components and migrating and nonmigrating tidal composites. The results reveal significant seasonal variations in the thermosphere amplitudes of DW1, SW2, and DE2. By comparing the seasonal variations and zonal distribution of the lower atmospheric tides extracted from temperature observation by MRO/MCS, the DE2 tidal amplitude is most substantial in the tropics in the thermosphere and mesosphere and exhibits a stronger amplitude in the first half of the Martian year than that in the second half of the Martian year. In contrast, there are significant differences in the zonal distribution and seasonal variations of DW1 and SW2 amplitudes between the mesosphere and thermosphere.

By examining the vertical phase velocities of tides, it was found that among the 14 tidal components, only the tropical mean DE2 tide exhibits upward propagation in the thermosphere (100-150 km). The vertical propagation characteristics of DE2 are significant during the northern spring, summer, and autumn (from Ls 330° to 210°) in the northern hemisphere. The tidal excitation source can be traced downward to the lower atmosphere between 40 km and 70 km or even lower. However, near the perihelion (from Ls 210° to 270°), the upward propagation of DE2 tides in the thermospheric atmosphere is suppressed. The seasonal variations in the vertical propagation of DE2 agree closely with the (1, 1) Hough mode. Still, they are inconsistent with the (1, 3) Hough mode, which exhibits noticeable upward propagation near the perihelion (Ls 150° to 270°). As the first antisymmetric mode, the (1, 2) mode can only propagate upward to ~130 km from Ls 150° to 270°.

In conclusion, our findings indicate that specific thermal tides (DE2) on Mars can propagate upward from the lower atmosphere to the thermosphere beyond 150 km. This upward propagation facilitates the energy and momentum transfer from the lower to the upper atmosphere, potentially influencing the vertical coupling within the Martian atmospheric layers. As activities in the Martian lower atmosphere, like dust storms, may impact the upper atmosphere through tides and other waves (Wu, Li, Heavens, et al., 2022; Yiğit, 2021), the DE2 tide could play a critical role in the climate evolution, affecting processes such as water vapor transport and atmospheric escape across the entire Martian atmosphere.

Acknowledgments

This work was supported by the B-type Strategic Priority Program of the Chinese Academy of Sciences, Grant XDB41000000; the National Natural Science Foundation of China grants (42275133, 42130203, 42241115, 42241135, 41874180, 41974175, and 41831071); the preresearch project on Civil Aerospace Technologies no. D020105 funded by China's National Space.

Open Research

Data Availability Statement

The MAVEN/IUVS calibrated (level 1B) stellar occultation data (Schneider, 2022) are publicly available in FITS format on the NASA Planetary Data System (PDS) at https://atmos.nmsu.edu/PDS/data/PDS4/MAVEN/iuvs_ calibrated_bundle/l1b/occultation/, identified by "occultation" with version/revision tag v13_r01. Data used in this study, can be downloaded from the CU Scholar data repository (Gupta, 2022) at https://scholar.colorado.edu/concern/datasets/h702q775d. The derived diurnal and semidiurnal tidal amplitude and phase from MAVEN/IUVS and MRO/MCS can be accessed on OSF repository (Yang et al., 2023)

References

Angelats I Coll, M., Forget, F., López-Valverde, M. A., Read, P. L., & Lewis, S. R. (2004). Upper atmosphere of Mars up to 120 km: Mars Global Surveyor accelerometer data analysis with the LMD general circulation model. *Journal of Geophysical Research: Planets*, *109*(E1), 2003JE002163. https://doi.org/10.1029/2003JE002163

Chapman, S., & Lindzen, R. S. (1987). *Atmospheric tides: Thermal and gravitational*. Gordon and Breach ; D. Reidel.

England, S. L., Liu, G., Kumar, A., Mahaffy, P. R., Elrod, M., Benna, M., Jain, S., Deighan, J., Schneider, N. M., McClintock, W. E., & Evans, J. S. (2019). Atmospheric Tides at High Latitudes in the Martian Upper Atmosphere Observed by MAVEN and MRO. *Journal of Geophysical Research: Space Physics*, *124*(4), 2943–2953. https://doi.org/10.1029/2019JA026601

England, S. L., Liu, G., Withers, P., Yiğit, E., Lo, D., Jain, S., Schneider, N. M., Deighan, J., McClintock, W. E., Mahaffy, P. R., Elrod, M., Benna, M., & Jakosky, B. M. (2016). Simultaneous observations of atmospheric tides from combined in situ and remote observations at Mars from the MAVEN spacecraft. *Journal of Geophysical Research: Planets*, *121*(4), 594–607. https://doi.org/10.1002/2016JE004997

Forbes, J. M. (2013). Tidal and Planetary Waves. In R. M. Johnson & T. L. Killeen (Eds.), *Geophysical Monograph Series* (pp. 67–87). American Geophysical Union. https://doi.org/10.1029/GM087p0067

Forbes, J. M., Bridger, A. F. C., Bougher, S. W., Hagan, M. E., Hollingsworth, J. L., Keating, G. M., & Murphy, J. (2002). Nonmigrating tides in the thermosphere of Mars. *Journal of Geophysical Research: Planets*, *107*(E11). https://doi.org/10.1029/2001JE001582

Forbes, J. M., Zhang, X., Forget, F., Millour, E., & Kleinböhl, A. (2020). Solar Tides in the Middle and Upper Atmosphere of Mars. *Journal of Geophysical Research: Space Physics*, *125*(9), e2020JA028140. https://doi.org/10.1029/2020JA028140

Fu, M., Ren, Z., Cui, J., Zhou, X., Wu, Z., & Fan, K. (2023). Atmospheric Tides at Low Latitudes in the Martian Upper Atmosphere Observed by MAVEN IUVS. *Journal of Geophysical Research: Space Physics*, *128*(10), e2023JA032016. https://doi.org/10.1029/2023JA032016

Gröller, H., Montmessin, F., Yelle, R. V., Lefèvre, F., Forget, F., Schneider, N. M., Koskinen, T. T., Deighan, J., & Jain, S. K. (2018). MAVEN/IUVS Stellar Occultation Measurements of Mars Atmospheric Structure and Composition. *Journal of Geophysical Research: Planets*, *123*(6), 1449–1483. https://doi.org/10.1029/2017JE005466

Gupta, S., Yelle, R. V., Schneider, N. M., Jain, S. K., González-Galindo, F., Verdier, L., Braude, A. S., Montmessin, F., Mayyasi, M., Deighan, J., & Curry, S. (2022). Thermal Structure of the Martian Upper Mesosphere/Lower Thermosphere From MAVEN/IUVS Stellar Occultations. *Journal of Geophysical Research: Planets*, *127*(11). https://doi.org/10.1029/2022JE007534

Hanel, R., Conrath, B., Hovis, W., Kunde, V., Lowman, P., Maguire, W., Pearl, J., Pirraglia, J., Prabhakara, C., Schlachman, B., Levin, G., Straat, P., & Burke, T. (1972). Investigation of the Martian environment by infrared spectroscopy on Mariner 9. *Icarus*, *17*(2), 423–442. https://doi.org/10.1016/0019-1035(72)90009-7

Jakosky, B. M., Lin, R. P., Grebowsky, J. M., Luhmann, J. G., Mitchell, D. F., Beutelschies, G., Priser, T., Acuna, M., Andersson, L., Baird, D., Baker, D., Bartlett, R., Benna, M., Bougher, S., Brain, D., Carson, D., Cauffman, S., Chamberlin, P., Chaufray, J.-Y., … Zurek, R. (2015). The Mars Atmosphere and Volatile Evolution (MAVEN) Mission. *Space Science Reviews*, *195*(1–4), 3–48. https://doi.org/10.1007/s11214-015-0139-x

Jiang, F. Y., Yelle, R. V., Jain, S. K., Cui, J., Montmessin, F., Schneider, N. M., Deighan, J., Gröller, H., & Verdier, L. (2019). Detection of Mesospheric CO_2 Ice Clouds on Mars in Southern Summer. *Geophysical Research Letters*, *46*(14), 7962–7971. https://doi.org/10.1029/2019GL082029

Kleinböhl, A., Schofield, J. T., Kass, D. M., Abdou, W. A., Backus, C. R., Sen, B., Shirley, J. H., Lawson, W. G., Richardson, M. I., Taylor, F. W., Teanby, N. A., & McCleese, D. J. (2009). Mars Climate Sounder limb profile retrieval of atmospheric temperature, pressure, and dust and water ice opacity. *Journal of Geophysical Research: Planets*, *114*(E10), 2009JE003358. https://doi.org/10.1029/2009JE003358

Lee, C., Lawson, W. G., Richardson, M. I., Heavens, N. G., Kleinböhl, A., Banfield, D., McCleese, D. J., Zurek, R., Kass, D., Schofield, J. T., Leovy, C. B., Taylor, F. W., & Toigo, A. D. (2009). Thermal tides in the Martian middle atmosphere as seen by the Mars Climate Sounder. *Journal of Geophysical Research: Planets*, *114*(E3), 2008JE003285. https://doi.org/10.1029/2008JE003285

McCleese, D. J., Schofield, J. T., Taylor, F. W., Calcutt, S. B., Foote, M. C., Kass, D. M., Leovy, C. B., Paige, D. A., Read, P. L., & Zurek, R. W. (2007). Mars Climate Sounder: An investigation of thermal and water vapor structure, dust and condensate distributions in the atmosphere, and energy balance of the polar regions. *Journal of Geophysical Research: Planets*, *112*(E5), 2006JE002790. https://doi.org/10.1029/2006JE002790

McClintock, W. E., Schneider, N. M., Holsclaw, G. M., Clarke, J. T., Hoskins, A. C., Stewart, I., Montmessin, F., Yelle, R. V., & Deighan, J. (2015). The Imaging Ultraviolet Spectrograph (IUVS) for the MAVEN Mission. *Space Science Reviews*, *195*(1–4), 75–124. https://doi.org/10.1007/s11214-014-0098-7

Moudden, Y., & Forbes, J. M. (2015). Density prediction in Mars' aerobraking region. *Space Weather*, *13*(1), 86–96. https://doi.org/10.1002/2014SW001121

Nakagawa, H., Jain, S. K., Schneider, N. M., Montmessin, F., Yelle, R. V., Jiang, F., Verdier, L., Kuroda, T., Yoshida, N., Fujiwara, H., Imamura, T., Terada, N., Terada, K., Seki, K., Gröller, H., & Deighan, J. I. (2020). A Warm Layer in the Nightside Mesosphere of Mars. *Geophysical Research Letters*, *47*(4), e2019GL085646. https://doi.org/10.1029/2019GL085646

Nakagawa, H., Terada, N., Jain, S. K., Schneider, N. M., Montmessin, F., Yelle, R. V., Jiang, F., Verdier, L., England, S. L., Seki, K., Fujiwara, H., Imamura, T., Yoshida, N., Kuroda, T., Terada, K., Gröller, H., Deighan, J., & Jakosky, B. M. (2020). Vertical Propagation of Wave Perturbations in the Middle Atmosphere on Mars by MAVEN/IUVS. *Journal of Geophysical Research: Planets*, *125*(9), e2020JE006481. https://doi.org/10.1029/2020JE006481

Shaposhnikov, D. S., Medvedev, A. S., Rodin, A. V., & Hartogh, P. (2019). Seasonal Water "Pump" in the Atmosphere of Mars: Vertical Transport to the Thermosphere. *Geophysical Research Letters*, *46*(8), 4161–4169. https://doi.org/10.1029/2019GL082839

Wilson, R. J. (2002). Evidence for nonmigrating thermal tides in the Mars upper atmosphere from the Mars Global Surveyor Accelerometer Experiment. *Geophysical Research Letters*, *29*(7). https://doi.org/10.1029/2001GL013975

Withers, P., Pratt, R., Bertaux, J.-L., & Montmessin, F. (2011). Observations of thermal tides in the middle atmosphere of Mars by the SPICAM instrument. *Journal of Geophysical Research*, *116*(E11), E11005. https://doi.org/10.1029/2011JE003847

Wu, Z., Li, T., Heavens, N. G., Newman, C. E., Richardson, M. I., Yang, C., Li, J., & Cui, J. (2022). Earth-like thermal and dynamical coupling processes in the Martian climate system. *Earth-Science Reviews*, *229*, 104023. https://doi.org/10.1016/j.earscirev.2022.104023

Wu, Z., Li, T., Li, J., Yang, C., & Cui, J. (2022). Diurnal Variations of Water Ice in the Martian Atmosphere Observed by Mars Climate Sounder. *Remote Sensing*, *14*(9), 2235. https://doi.org/10.3390/rs14092235

Wu, Z., Li, T., Li, J., Zhang, X., Yang, C., & Cui, J. (2021). Abnormal Phase Structure of Thermal Tides During Major Dust Storms on Mars: Implications for the Excitation Source of High-altitude Water Ice Clouds. *Journal of Geophysical Research: Planets*, *126*(4), e2020JE006758. https://doi.org/10.1029/2020JE006758

Wu, Z., Li, T., Zhang, X., Li, J., & Cui, J. (2020). Dust tides and rapid meridional motions in the Martian atmosphere during major dust storms. *Nature Communications*, *11*(1), 614. https://doi.org/10.1038/s41467-020-14510-x

Yang, C., Li, T., Yuan, M.,& Wu, Z. (2023). Martian atmospheric tides revealed from MAVEN and MCS Observations [Dataset]. OSF. https://doi.org/10.17605/OSF.IO/S8XU5

Yiğit, E. (2021). Martian water escape and internal waves. *Science*, *374*(6573), 1323–1324. https://doi.org/10.1126/science.abg5893

Yiğit, E. (2023). Coupling and interactions across the Martian whole atmosphere system. *Nature Geoscience*, *16*(2), 123–132. https://doi.org/10.1038/s41561-022-01118-7

Figure 1.

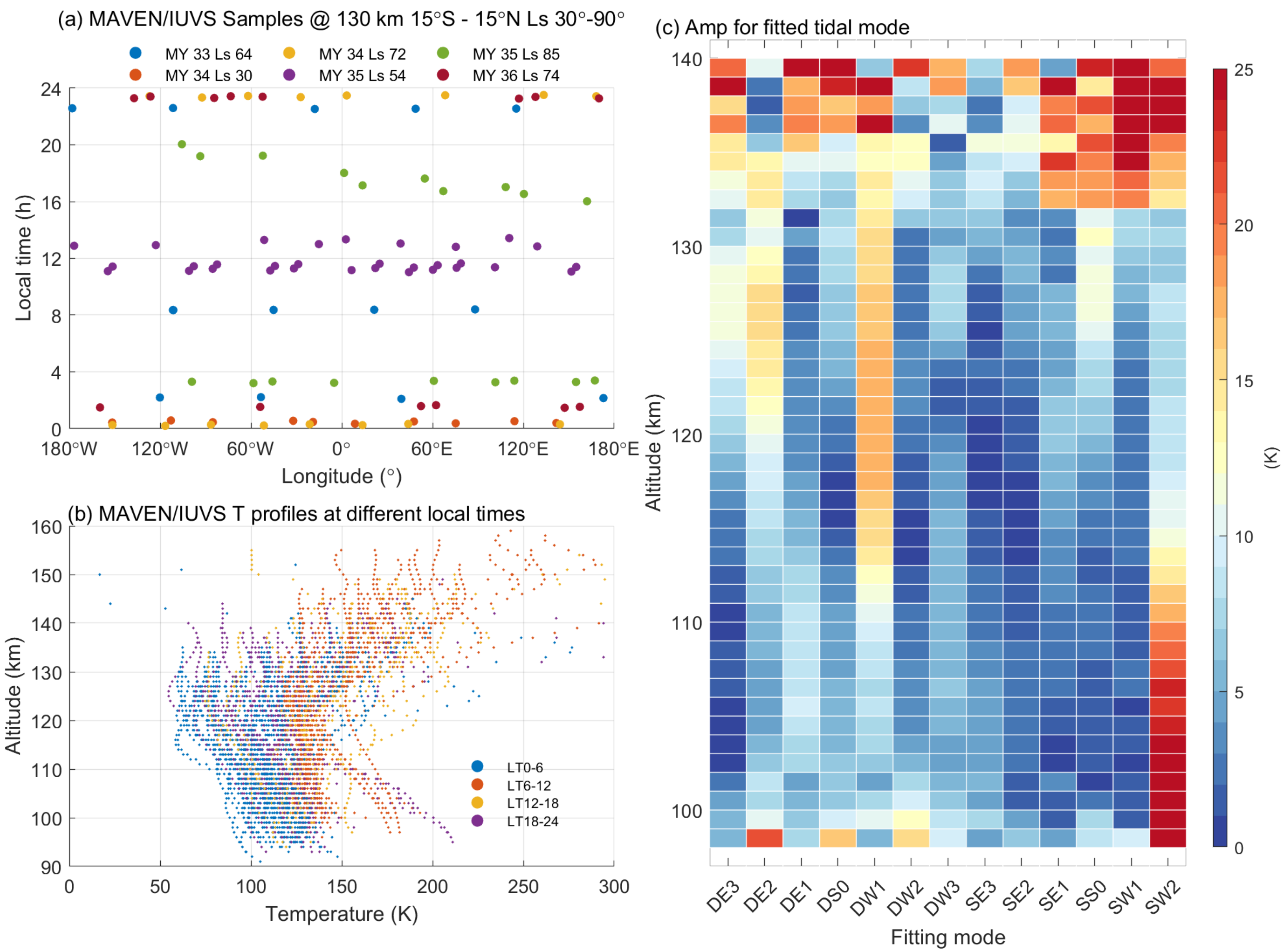
(a) MAVEN/IUVS Samples @ 130 km 15°S - 15°N Ls 30°-90°
MY 33 Ls 64
MY 34 Ls 30
MY 34 Ls 72
MY 35 Ls 54
MY 35 Ls 85
MY 36 Ls 74
Local time (h)
Longitude (°)
180°W
120°W
60°W
0°
60°E
120°E
180°E
(b) MAVEN/IUVS T profiles at different local times
LT0-6
LT6-12
LT12-18
LT18-24
Altitude (km)
Temperature (K)
(c) Amp for fitted tidal mode
DE3
DE2
DE1
DS0
DW1
DW2
DW3
SE3
SE2
SE1
SS0
SW1
SW2
Fitting mode
(K)

Figure 2.

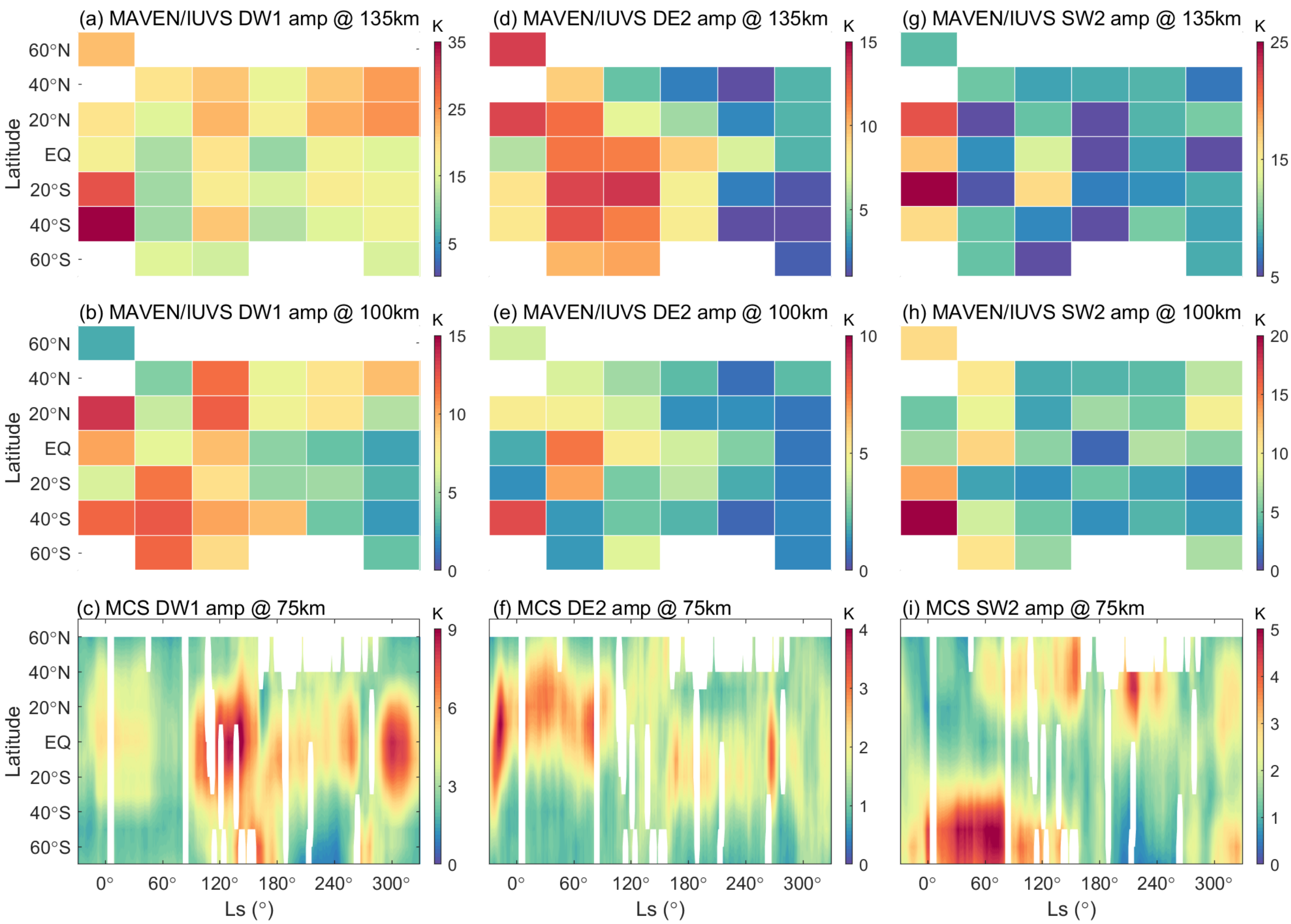
(a) MAVEN/IUVS DW1 amp @ 135km
(d) MAVEN/IUVS DE2 amp @ 135km
(g) MAVEN/IUVS SW2 amp @ 135km
(b) MAVEN/IUVS DW1 amp @ 100km
(e) MAVEN/IUVS DE2 amp @ 100km
(h) MAVEN/IUVS SW2 amp @ 100km
(c) MCS DW1 amp @ 75km
(f) MCS DE2 amp @ 75km
(i) MCS SW2 amp @ 75km
Latitude
60°N
40°N
20°N
EQ
20°S
40°S
60°S
Ls (°)
0°
60°
120°
180°
240°
300°
K

Figure 3.

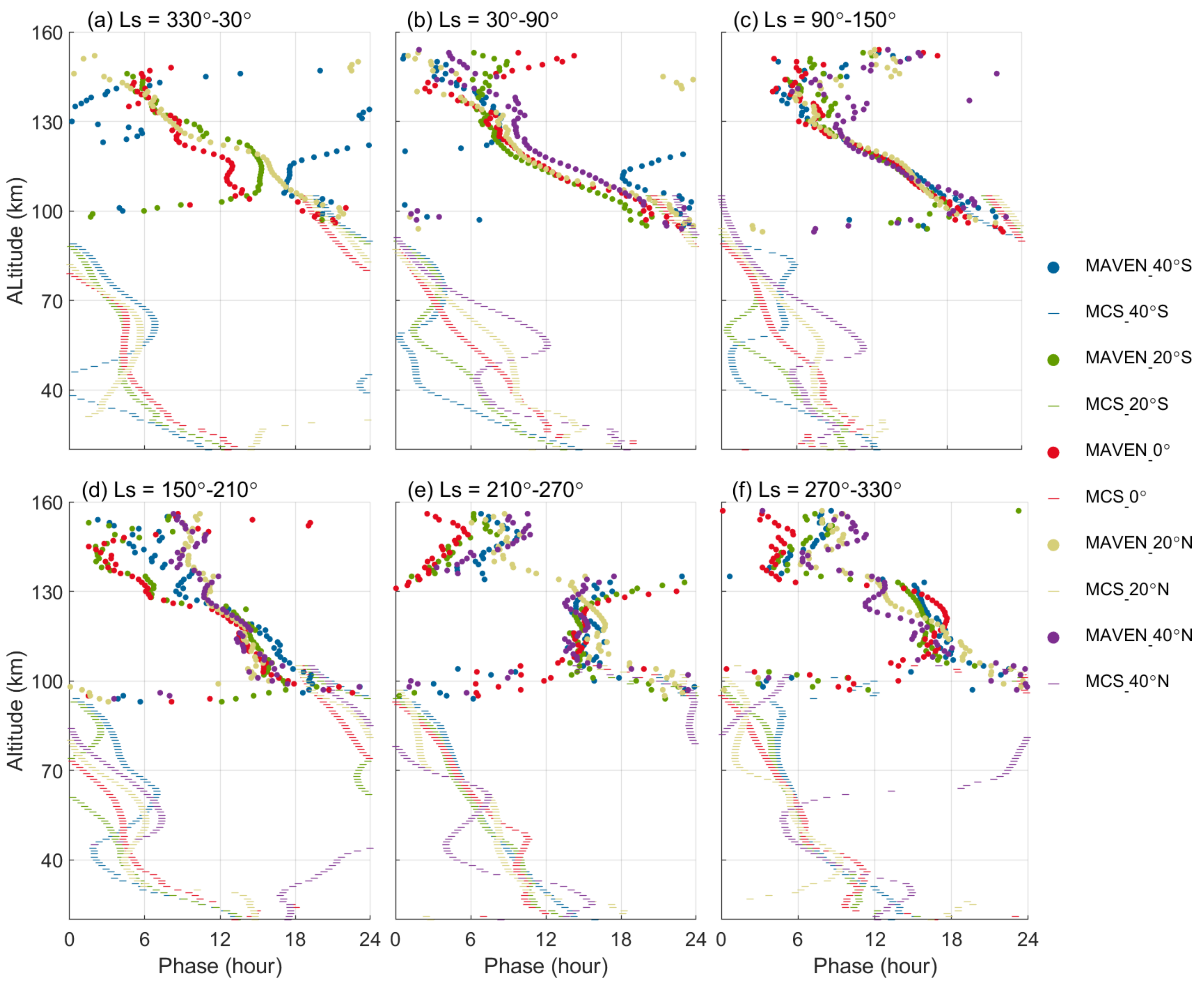

(a) Ls = 330°-30°
(b) Ls = 30°-90°
(c) Ls = 90°-150°
(d) Ls = 150°-210°
(e) Ls = 210°-270°
(f) Ls = 270°-330°
ALtitude (km)
Altitude (km)
Phase (hour)
MAVEN_40°S
MCS_40°S
MAVEN_20°S
MCS_20°S
MAVEN_0°
MCS_0°
MAVEN_20°N
MCS_20°N
MAVEN_40°N
MCS_40°N

Figure 4.

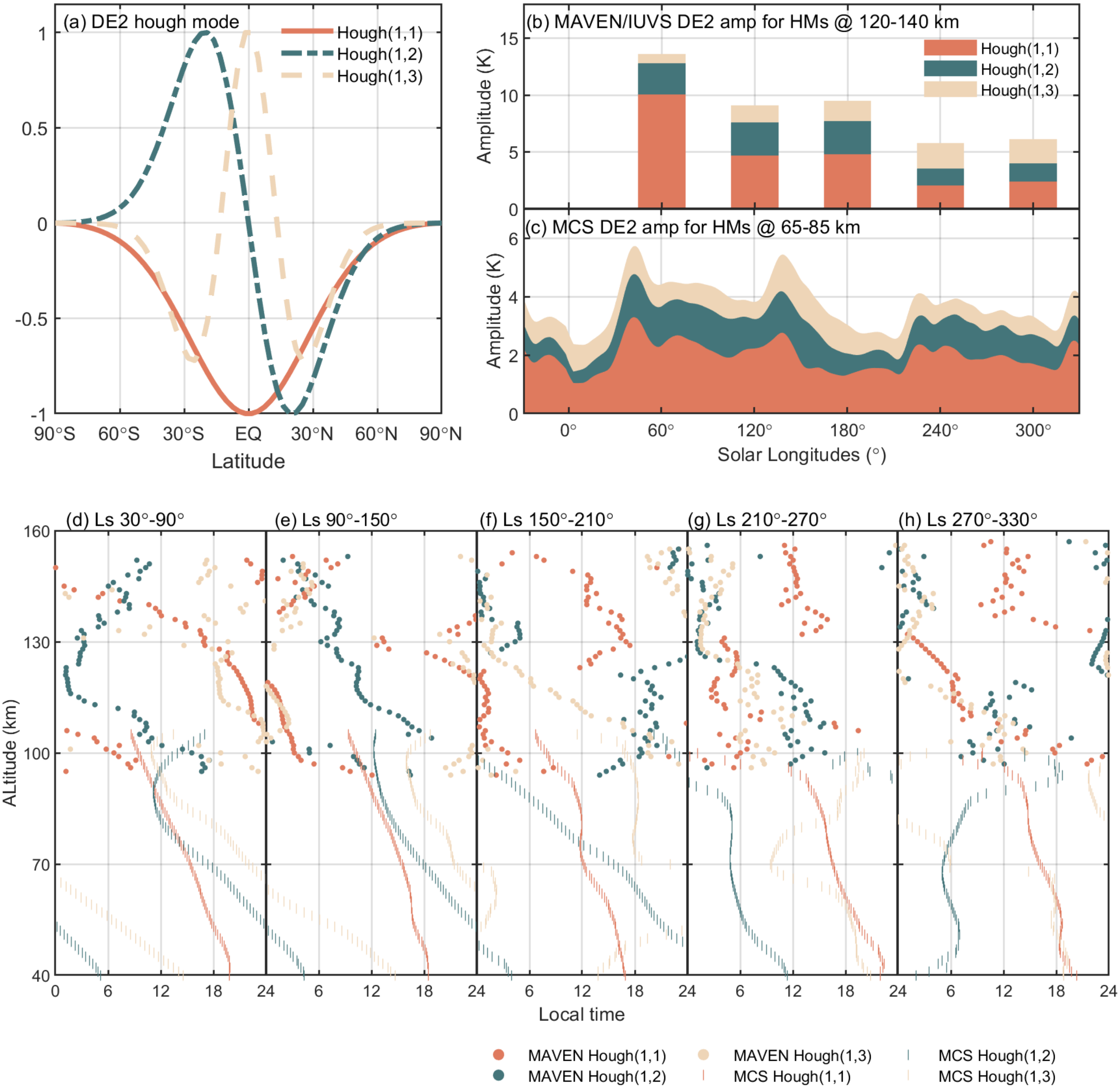

(a) DE2 hough mode
Hough(1,1)
Hough(1,2)
Hough(1,3)
90°S 60°S 30°S EQ 30°N 60°N 90°N
Latitude
(b) MAVEN/IUVS DE2 amp for HMs @ 120-140 km
Amplitude (K)
(c) MCS DE2 amp for HMs @ 65-85 km
Solar Longitudes (°)
(d) Ls 30°-90°
(e) Ls 90°-150°
(f) Ls 150°-210°
(g) Ls 210°-270°
(h) Ls 270°-330°
ALtitude (km)
Local time
MAVEN Hough(1,1)
MAVEN Hough(1,2)
MAVEN Hough(1,3)
MCS Hough(1,1)
MCS Hough(1,2)
MCS Hough(1,3)